THE JOURNAL OF PHYSICAL CHEMISTRY C

Article

pubs.acs.org/JPCC

Unexpectedly Fast Phonon-Assisted Exciton Hopping between Carbon Nanotubes

A. H. Davoody,*,† F. Karimi,† M. S. Arnold,‡ and I. Knezevic*,†

†Department of Electrical and Computer Engineering and ‡Department of Materials Science and Engineering, University of Wisconsin—Madison, Madison, Wisconsin 53706-1691, United States

ABSTRACT: Carbon-nanotube (CNT) aggregates are promising light-absorbing materials for photovoltaics. The hopping rate of excitons between CNTs directly affects the efficiency of these devices. We theoretically investigate phonon-assisted exciton hopping, where excitons scatter with phonons into a same-tube transition state, followed by intertube Coulomb scattering into the final state. Second-order hopping between bright excitonic states is as fast as the first-order process (~1 ps). For perpendicular CNTs, the high rate stems from the high density of phononic states; for parallel CNTs, the reason lies in relaxed selection rules. Moreover, second-order exciton transfer between dark and bright states, facilitated by phonons with large angular momentum, has rates comparable to bright-to-bright transfer, so dark excitons provide an additional pathway for energy transfer in CNT composites. As dark excitons are difficult to probe in experiment, predictive theory is critical for understanding exciton dynamics in CNT composites.

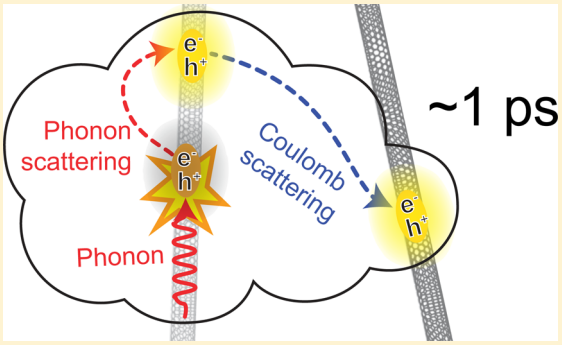

1. INTRODUCTION

Carbon nanotubes (CNTs) are presently garnering attention for potential use in photovoltaic solar-cell and photodetector applications.[1−10] The development of these CNT-based photovoltaics is dependent on the photophysics of CNTs. In the past two decades, there has been considerable improvement in our understanding of the electronic and optical properties of CNTs, with a special effort to isolate and study the properties of individual CNTs.[11] However, the physical processes that are important in determining the efficiency of photovoltaic devices depend on the electronic interactions *between* CNTs. An example of these processes is intertube exciton hopping, which is directly related to the efficiency of photovoltaics that use CNTs as the light absorber. Therefore, it is critical to understand the mechanisms through which excitons hop between CNTs and to maximize the intertube exciton-transfer (ET) rate.[12]

In recent years, several groups have measured the intertube ET rate in CNT films.[13−22] The reported results range from tens of femtoseconds to tens of picoseconds. In our recent paper,[23] we calculated the ET rate between pairs of semiconducting CNTs using first-order Fermi's golden rule

$$S^{(1)}(i \to f) = \frac{2\pi}{\hbar} |\langle f|V|i\rangle|^2 \, \delta(E_i - E_f) \tag{1}$$

We studied the effects of CNT chirality, exciton confinement, exciton scattering from impurities, and the relative orientation of the donor and acceptor CNTs. (The donor/acceptor CNT refers to the tube that hosts the electron before/after exciton transfer.) We showed that the origins of the wide range of measured ET rates are exciton confinement in local quantum wells that stems from disorder and exciton thermalization between bright and dark excitonic states. The physical process behind this type of exciton hopping is elastic: exciton hopping happens via Coulomb coupling between the initial and final excitonic states with equal energies. The phonon baths within each CNT act as intratube scattering sources and help relax exciton populations toward thermal equilibrium. Therefore, phonons play an indirect role in the first-order ET process.

Several studies have shown that ET between molecules and quantum dots can be facilitated by higher-order processes, which include exciton−phonon interactions.[24−31] In these types of processes, the underlying phonon bath plays a *direct* role in the ET process. Rebentrost et al. studied the effect of the exciton−phonon coupling strength on the efficiency and rate of ET in quantum dots.[29] They showed that there is an optimal range of exciton−phonon coupling strengths that leads to an increase in the ET rate; in this range, exciton−phonon scattering rates are comparable to typical excitonic energy spacings (in the units of $\hbar$). However, these findings are not directly applicable to CNTs, where the energy levels have smaller spacings than the quasi-zero-dimensional molecular systems and quantum dots.[25] Recently, Postupna et al.[32] used a molecular-dynamics technique along with density functional theory to show that exciton−phonon coupling could change the band structure and symmetry of dark excitons, thereby opening new pathways for ET between arrays of carbon nanotubes.

Received: April 27, 2017
Revised: June 3, 2017
Published: June 5, 2017

DOI: 10.1021/acs.jpcc.7b03994
J. Phys. Chem. C 2017, 121, 13084−13091

In this paper, we present a calculation of the phonon-assisted ET rates using second-order Fermi's golden rule. This transfer process consist of two successive scattering events: intratube scattering of excitons due to their interaction with phonons, followed by intertube scattering of excitons due to Coulomb coupling between the two CNTs (or vice versa—intertube first, intratube second). The excitonic states in CNTs are calculated by solving the Bethe−Salpeter equation in the basis of tight-binding single-particle states.[33,34] Band bending due to the presence of neighboring CNTs is on the order of a few tens of meVs,[32,35] which is small when compared to the band gap difference for the CNTs considered here and is therefore neglected. The exciton−phonon interactions are calculated using the Su−Schrieffer−Heeger (SSH) model.[36,37] The Coulomb coupling between excitonic states is calculated within the transition-monopole approximation (TMA).[23,38,39]

Our results show that the second-order phonon-assisted ET process between CNTs has a rate of about 1 ps^{-1}, which is the same order of magnitude as the first-order ET process. The reason behind this fast second-order process depends on the orientation of the donor and acceptor tubes: (1) When the CNTs are nonparallel, the large density of the phononic states that facilitate the ET process causes the high transfer rates. (2) When the CNTs are parallel, the participation of phononic states helps with finding the initial and final quantum states that simultaneously conserve momentum and energy, thereby increasing the number of suitable donor and acceptor excitonic states, which leads to high rates of phonon-assisted ET. We also find that, for optically inactive *E*-type excitons, the phonon-assisted transfer rate (~1 ps^{-1}) is at least 2 orders of magnitude higher than the rate of the first-order transfer process (~0.01 ps^{-1}). These results are important from an experimental point of view, as optically inactive excitons are invisible in the most common measurement methods (time-resolved photoluminescence spectroscopy and pump−probe spectroscopy), so one needs to complement measurements with theoretical calculations in order to get a complete picture of exciton dynamics in these types of nanostructures.

2. THEORY OF PHONON-ASSISTED EXCITON TRANSFER

According to Fermi's golden rule,[40] the second-order transition rate is given by

$$S^{(2)}(i \to f) = \frac{2\pi}{\hbar} \left| \sum_m \frac{\langle f|V|m\rangle\langle m|V|i\rangle}{E_i - E_m + i\gamma} \right|^2 \delta(E_i - E_f) \tag{2}$$

where the electronic system is initially in state $|i\rangle$ and is in state $|f\rangle$ after transfer. $|m\rangle$ is an intermediate state that the electronic system jumps into as the first step of the scattering process and jumps out of (and into the state $|f\rangle$) in the second step. A schematic of second-order scattering is shown in Figure 1. γ is the lifetime of the initial state, $|i\rangle$, which will be discussed later. Scattering is caused by a perturbation Hamiltonian (V), which consists of exciton−phonon interaction (H_{ex-ph}) and the Coulomb interaction (H_{coul}) between the electrons in the donor and acceptor CNTs

$$V = H_{coul} + H_{ex-ph,1} + H_{ex-ph,2} \tag{3}$$

Indices 1 and 2 in the exciton−phonon interaction Hamiltonians refer to CNTs 1 and 2 because the phonon bath inside each CNT interacts only with excitons inside that CNT and can only result in intratube exciton scattering.

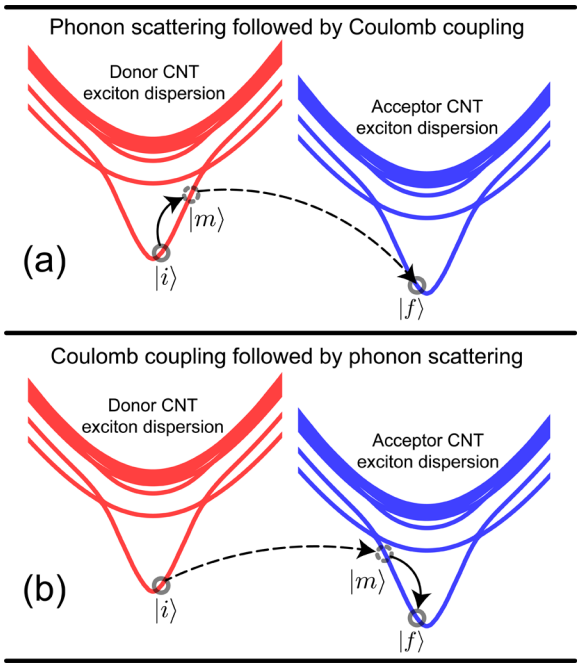

Figure 1. Second-order exciton scattering. Panel (a) shows exciton hopping where intratube exciton−phonon scattering is followed by intertube exciton scattering due to Coulomb interaction. Panel (b) shows exciton hopping where intertube exciton scattering due to Coulomb interaction is followed by intratube exciton−phonon scattering. Black dashed lines represent Coulomb scattering, while black solid lines represent scattering due to exciton−phonon interaction. Solid red and blue curves show the exciton energy dispersions in the donor and acceptor CNTs, respectively.

The radial breathing modes (RBMs) in CNTs couple weakly with excitons, so the graphene-like G modes dominate exciton−phonon interaction.[37,41] As the RBM modes are of little importance here, for numerical simplicity, we calculate phonon dispersions by zone folding of graphene modes,[42] which is an accurate approach for G modes.

The exciton−phonon interaction Hamiltonian in the *i*-th CNT is

$$H_{ex-ph,i} = \frac{1}{\sqrt{L_i}} \sum_{s,s'} \sum_{\lambda} \sum_{\mathbf{K},\mathbf{q}} g_{iss'}(\lambda, \mathbf{q}, \mathbf{K}) \times \cdots$$
$$\cdots (c^{\dagger}_{i,\lambda}(\mathbf{q}) + c_{i,\lambda}(-\mathbf{q})) \left| i, s', \mathbf{K} - \frac{\mathbf{q}}{2} \right\rangle \langle i, s, \mathbf{K}| \tag{4}$$

where $c^{\dagger}_{i,\lambda}(\mathbf{q})$ and $c_{i,\lambda}(\mathbf{q})$ are the phonon creation and annihilation operators in the *i*-th CNT, respectively. $\mathbf{q}$ is the phonon wave vector, and λ is the phonon branch index. $|i,s,\mathbf{K}\rangle$ is the state with a single exciton in the *i*-th CNT. Here, we limit ourselves to the cases where only one CNT is excited and hosts a single exciton, while the other CNTs are in the ground state. The single-exciton approximation is appropriate for low-intensity illumination conditions, common in experiment.[19,20]

$\mathbf{K}$ is the wave vector of the exciton center-of-mass, and s is a quantum number analogous to the principal quantum number in a hydrogen atom. L_i is the CNT length. $g_{ss'}(\lambda, \mathbf{q}, \mathbf{K})$ is the exciton−phonon coupling term given by the Su−Schrieffer−Heeger (SSH) model,[36,37] which is appropriate for the coupling of excitons with G phonon modes. In the SSH model, the tight-

DOI: 10.1021/acs.jpcc.7b03994
J. Phys. Chem. C 2017, 121, 13084−13091

binding matrix element $t = t_0 - g\delta u$ is modulated by the longitudinal displacement of nearest-neighbor atoms (δu) owing to phonon vibrations. The electron−phonon coupling constant in CNTs is g = 5.3 eV/Å.[37]

Unlike the exciton−phonon interaction, which only results in intratube exciton scattering, the Coulomb coupling Hamiltonian

$$H_{\text{coul}} = \sum_{\mathbf{K},s} \sum_{\mathbf{K}',s'} M(\mathbf{K}, s; \mathbf{K}', s')|2, s', \mathbf{K}'\rangle\langle 1, s, \mathbf{K}| + \text{h.c.} \tag{5}$$

is responsible for intertube exciton scattering. The Coulomb coupling matrix element, M, is calculated under the TMA[23] and shows two different types of behavior, depending on whether the donor and acceptor CNTs are parallel or not. Both cases are present in most processed CNT samples, as the CNTs tend to form bundles in which the tubes are parallel and the CNT bundles are randomly oriented with respect to one another. We will discuss the cases of both parallel and nonparallel CNTs.

In the following, we discuss second-order exciton hopping between pairs of perpendicular and parallel CNTs for the two types of hopping process shown in Figure 1: (i) exciton−phonon scattering within the donor CNT followed by Coulomb scattering into the final state in the acceptor CNT (Figure 1a) and (ii) Coulomb scattering from the initial state in the donor CNT into an intermediate state in the acceptor CNT, followed by exciton−phonon scattering within the acceptor CNT (Figure 1b). Both (i) and (ii) can involve emission or absorption of a phonon [see eq 4], with emission being the dominant (higher-rate) process. Therefore, we consider only phonon emission in the rest of the paper.

As an aside, we also note that a type-II heterojunction and the resulting dissociation and charge transfer can happen when tubes are in very close proximity and have large orbital overlap. However, typical intertube surface distances in experiment are no less than 5 Å,[20] owing to surface charge and polymer residue left over from the process of separation of semiconductor nanotubes from the CNT soot. For typical distances, Postupna et al.[32] have shown, using *ab initio* calculations, that the energy transfer phenomena (i.e., exciton transfer) are dominant, as they happen considerably faster than charge transfer (i.e., dissociation of excitons into electrons and holes).

2.1. Perpendicular CNTs. When the CNTs are nonparallel, the Coulomb matrix element is inversely dependent on the length of donor (L_1) and acceptor (L_2) CNTs

$$M(s, \mathbf{K}; s', \mathbf{K}') = \frac{1}{\sqrt{L_1 L_2}} M_\perp(s, \mathbf{K}; s', \mathbf{K}') \tag{6}$$

This length dependence can be understood by realizing that the average distance between the CNTs increases with increasing length of the CNTs, which results in weaker Coulomb coupling between longer tubes. Here, $M_\perp$ is a length-independent Coulomb matrix element; it is the term remaining after the length dependence is explicitly pulled out of the full matrix element $M(s, K; s', K')$ in eq 6. We also note that, when the donor and acceptor CNTs are nonparallel, the exciton center-of-mass momentum does not have to be conserved in the exciton hopping process.

We calculate the total ET rate for a unit length of donor CNT by summing the transition rate for every possible phononic (λ and $\mathbf{q}$) and final excitonic state (s_2 and $\mathbf{K}_2$). For perpendicular tubes, the rate for a unit length of a donor CNT is a quantity important in experiment, as one often measures the rate of scattering from a donor CNT to a bundle of acceptor CNTs, all of which cross the donor tube, so the actual length of one crossing and the density of acceptor tubes are important in obtaining the final rates (see a detailed discussion in refs 23 and 43). The expressions for the ET rate through second-order process types (i) and (ii) together (shown in Figures 1a and 1b, respectively) are similar, with some differences in the selection rules for the transition and final states. For process type (i), the total ET rate from a donor CNT of unit length to a set of acceptor CNTs that are perpendicular to the donor is given by

$$\begin{aligned}\tilde{\Gamma}(s_1, \mathbf{K}_1) &= L_1 \times \sum_{s_2,\mathbf{K}_2} \sum_{\lambda,\mathbf{q}} S(s_1, \mathbf{K}_1 \to s_2, \mathbf{K}_2, \lambda, \mathbf{q}) \\ &= \frac{1}{2\pi\hbar} \sum_{s_2,\mathcal{M}_2} \sum_{\lambda,\mu} \int dK_2 \frac{n_{1,\lambda}(\mathbf{q}_0) + 1}{|\hbar\dot{\omega}_{1,\lambda}(\mathbf{q}_0)|} \\ &\times \left| \sum_{s'} \frac{g_{1s_1s'}(\lambda, \mathbf{q}_0, \mathbf{K}_1) M_\perp\left(\mathbf{K}_1 - \frac{\mathbf{q}_0}{2}, s'; \mathbf{K}_2, s_2\right)}{\Omega_{1,s_1}(\mathbf{K}_1) - \Omega_{1,s'}\left(\mathbf{K}_1 - \frac{\mathbf{q}_0}{2}\right) - \hbar\omega_{1,\lambda}(\mathbf{q}_0) + i\gamma} \right|^2 \end{aligned} \tag{7}$$

For process type (ii), the corresponding rate is

$$\begin{aligned}\tilde{\Gamma}(s_1, \mathbf{K}_1) &= L_1 \times \sum_{s_2,\mathbf{K}_2} \sum_{\lambda,\mathbf{q}} S(s_1, \mathbf{K}_1 \to s_2, \mathbf{K}_2, \lambda, \mathbf{q}) \\ &= \frac{1}{2\pi\hbar} \sum_{s_2,\mathcal{M}_2} \sum_{\lambda,\mu} \int dK_2 \frac{n_{2,\lambda}(\mathbf{q}_0) + 1}{|\hbar\dot{\omega}_{2,\lambda}(\mathbf{q}_0)|} \\ &\times \left| \sum_{s'} \frac{\tilde{M}\left(\mathbf{K}_1, s_1; \mathbf{K}_2 + \frac{\mathbf{q}_0}{2}, s'\right) \tilde{g}_{2s's_2}\left(\lambda, \mathbf{q}_0, \mathbf{K}_2 + \frac{\mathbf{q}_0}{2}\right)}{\Omega_{1,s_1}(\mathbf{K}_1) - \Omega_{2,s'}\left(\mathbf{K}_2 + \frac{\mathbf{q}_0}{2}\right)} \right|^2 \end{aligned} \tag{8}$$

In eqs 7 and 8, $\Omega_{i,s}(\mathbf{K})$ is the exciton energy in the i-th CNT obtained by solving the Bethe−Salpeter equation.[23] $\hbar\omega_{1,\lambda}(\mathbf{q})$ is the energy of the emitted phonon in the donor CNT.[42] $n_{i,\lambda}(\mathbf{q}_0)$ is the thermal (Bose−Einstein) occupation number of phonons in tube i, branch λ, and with wave vector $\mathbf{q}_0$ at temperature T: $n_{i,\lambda}(\mathbf{q}_0) = (\exp(\hbar\omega_{i,\lambda(\mathbf{q}_0)}/k_B T) - 1)^{-1}$, where k_B is the Boltzmann constant. γ = 30 meV is the inverse lifetime due to the exciton−phonon scattering rate.[37,44,45] The phonon wave vector $\mathbf{q}_0$ is the value for which the energy is conserved in the exciton hopping process: $\Omega_{2,s_2}(\mathbf{K}_2) = \Omega_{1,s_1}(\mathbf{K}_1) - \hbar\omega_{1,\lambda}(\mathbf{q}_0)$. $\mathcal{M}$ and μ are the circumferential components of exciton and phonon wave vectors, respectively. In the SSH interaction term, g = 5.3 eV/Å and t_0 = 3.033 eV.[42] [Excitons with zero angular momentum ($\mathcal{M} = 0$) are called A-type excitons, which are further divided into the optically inactive (dark) A_1 and optically active (bright) A_2 excitons. Excitons with nonzero angular momentum ($\mathcal{M} \neq 0$) are dark and referred to as E-type. The first-order ET rate due to Coulomb coupling is generally 2 orders of magnitude higher among A_2 excitons than the ET rate between E-type and A_2 excitons.[23] Owing to symmetry, A_1 excitons do not contribute to exciton hopping via first- or second-order processes and will not be discussed here.]

It is important to note that the second-order ET rate between nonparallel CNTs [eq 7] contains the phonon density of states

DOI: 10.1021/acs.jpcc.7b03994
J. Phys. Chem. C 2017, 121, 13084−13091

$$\frac{1}{|\hbar\dot{\omega}_{n,\lambda}(\mathbf{q})|} = \left(\hbar\frac{\partial\omega_{n,\lambda}(\mathbf{q})}{\partial q}\right)^{-1} \tag{9}$$

which would be absent in phonon-assisted second-order processes between parallel tubes [see eq 11]. Namely, in most cases of phonon-assisted processes, the degree of freedom over the phonon wave vector is eliminated by momentum conservation, which results in a dependence of the rate on the electronic density of states. Once the momentum conservation is relaxed because of tube misorientation, the phonon density of states remains in the expression, and since it is much higher than the electronic density of states, we expect a much higher rate of the phonon-assisted second-order process between nonparallel than between parallel CNTs.[31]

2.2. Parallel CNTs. In the case of parallel CNTs, the Coulomb matrix element does not depend on the length of the CNTs, but instead it conserves the center-of-mass momentum

$$M(s, \mathbf{K}; s', \mathbf{K}') = \delta_{K,K'} \times M_{||}(s, \mathbf{K}; s', \mathbf{K}') \tag{10}$$

Here, $\delta_{K,K'}$ is the Kronecker delta function, which eliminates the phonon degree of freedom in the scattering process. The ET rate between two parallel CNTs due to process type (i) is

$$\begin{aligned}\Gamma(s_1, \mathbf{K}_1) &= \sum_{s_2,\mathbf{K}_2}\sum_{\lambda,\mathbf{q}} S(s_1, \mathbf{K}_1 \to s_2, \mathbf{K}_2, \lambda, \mathbf{q}) \\ &= \frac{1}{\hbar}\sum_{s_2,\mathbf{K}_{2,0}}\sum_{\lambda,\mu}\frac{n_{1,\lambda}(\mathbf{q}_0)+1}{\left|\frac{1}{2}\dot{\Omega}_{2,s_2}(\mathbf{K}_{2,0}) - \hbar\dot{\omega}_{1,\lambda}(\mathbf{q}_0)\right|} \\ &\times \left|\sum_{s'}\frac{g_{1s_1s'}(\lambda, \mathbf{q}_0, \mathbf{K}_1)M_{||}\left(\mathbf{K}_1 - \frac{\mathbf{q}_0}{2}, s'; \mathbf{K}_{2,0}, s_2\right)}{\Omega_{1,s_1}(\mathbf{K}_1) - \Omega_{1,s'}\left(\mathbf{K}_1 - \frac{\mathbf{q}_0}{2}\right) - \hbar\omega_{1,\lambda}(\mathbf{q}_0) + i\gamma}\right|^2\end{aligned} \tag{11}$$

For process type (ii), the expression is

$$\begin{aligned}\Gamma(s_1, \mathbf{K}_1) &= \frac{1}{\hbar}\sum_{s_2,\mathbf{K}_{2,0}}\sum_{\lambda,\mu}\frac{n_{2,\lambda}(\mathbf{q}_0)+1}{\left|\frac{1}{2}\dot{\Omega}_{2,s_2}(\mathbf{K}_{2,0}) - \hbar\dot{\omega}_{2,\lambda}(\mathbf{q}_0)\right|} \\ &\times \left|\sum_{s'}\frac{M_{||}\left(\mathbf{K}_1, s_1; \mathbf{K}_{2,0} + \frac{\mathbf{q}_0}{2}, s'\right)\tilde{g}_{2s's_2}\left(\lambda, \mathbf{q}_0, \mathbf{K}_{2,0} + \frac{\mathbf{q}_0}{2}\right)}{\Omega_{1,s_1}(\mathbf{K}_1) - \Omega_{2,s'}\left(\mathbf{K}_{2,0} + \frac{\mathbf{q}_0}{2}\right)}\right|^2\end{aligned} \tag{12}$$

Here, $\mathbf{K}_{2,0}$ and $\mathbf{q}_0$ are the wave vector of excitonic and phononic states which simultaneously conserve energy and momentum: $\Omega_{2,s_2}(\mathbf{K}_{2,0}) = \Omega_{1,s_1}(\mathbf{K}_1) - \hbar\omega_{1,\lambda}(\mathbf{q}_0)$, $\mathbf{K}_{2,0} = \mathbf{K}_1 - \frac{\mathbf{q}_0}{2}$.

In the case of parallel CNTs, the phonon density of states is absent due to the momentum-conservation requirement; therefore, in contrast to the perpendicular case, the phonon-assisted ET rate between parallel tubes does not benefit from the large density of phononic states.

3. RESULTS AND DISCUSSION

3.1. Phonon-Assisted Exciton Transfer Rate for Perpendicular CNTs. Figure 2a shows the phonon-assisted ET rates among A_2 excitonic states in perpendicular CNTs. The ET happens through phonon scattering within the donor CNT followed by the Coulomb coupling of the transition excitonic state in the donor CNT to the final excitonic state in the acceptor CNT. These second-order ET rates are within the range of measurements[13−22] and have the same order of magnitudes as the theoretical calculations of the first-order ET rates,[23] which makes them important from both experimental and theoretical points of view.

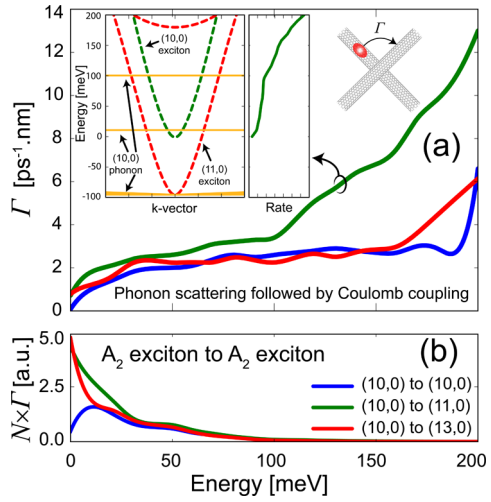

Figure 2. (a) Phonon-assisted ET rates between A_2 excitons in pairs of perpendicular CNTs via process type (i) (i.e., intratube phonon scattering followed by intertube Coulomb scattering). The energy axis starts from the bottom of the excitonic band in the donor CNT. (Left inset) Exciton band dispersions [green dashed line: (10,0) donor CNT; red dashed line: (11,0) acceptor CNT] and donor-CNT phonon dispersions (solid yellow horizontal lines). (Right inset) The ET rate, with the vertical energy axes aligned with that in the left inset, to emphasize the relationship between the onset of different phonon scattering channels and phonon dispersions. (b) Phonon-assisted ET rates multiplied by the thermal occupation number at temperature T = 300 K.

As we can see in Figure 2a, the ET rate increases with increasing exciton kinetic energy and depends on the chirality of the donor and acceptor tubes. In the case of CNT pairs with the same chirality [(10,0) → (10,0)], excitons with energies at the bottom of a band cannot emit a phonon (see blue curves in Figure 2), but the excitons with higher energies can. In the case of dissimilar chiralities, if the acceptor CNT has a smaller energy gap than the donor CNT [such as (10,0) → (11,0) or (10,0) → (13,0)], the excitons at the bottom of the dispersion curve can emit acoustic phonons, and the scattering rate is high (green and red curves in Figure 2b). As the exciton energy increases past a longitudinal-optical-phonon energy, we see a jump in the scattering rate due to the interaction of those optical phonons with excitons. The right inset in Figure 2 shows the scattering rate between (10,0) and (11,0) CNTs, with the same vertical energy scale as the left inset, which depicts the excitonic and phononic energy dispersions. We can see the turn-on of new exciton scattering pathways as the emission of new longitudinal optical phonon G-modes becomes possible.

However, the ET rate at the bottom of the band is of the greatest importance because the exciton occupation number decreases with increasing energy. Figure 2b shows the ET rate multiplied by the exciton thermal occupation number $N(\Omega) = \left(e^{-\beta\Omega}\frac{\partial K}{\partial\Omega}\right)/\mathcal{Z}$ where $\mathcal{Z}$ is the partition function and $\frac{\partial K}{\partial\Omega}$ is the exciton density of states at energy Ω. The effective ET rates measured in experiment are the areas under the curves in Figure 2b. These effective ET rates (summarized in Table 1) between CNTs with the same chirality are lower by a factor of 2 than the effective ET rates between pairs of CNTs with

DOI: 10.1021/acs.jpcc.7b03994
J. Phys. Chem. C 2017, 121, 13084−13091

Table 1. Effective Exciton Transfer Rates between Different Pairs of Perpendicular and Parallel Carbon Nanotubes at Temperature T = 300 K[a]

		(10,0) → (10,0)		(10,0) → (11,0)		(10,0) → (13,0)	
orientation	type	$A_2 \leftrightarrow A_2$	$E \leftrightarrow A_2$	$A_2 \leftrightarrow A_2$	$E \leftrightarrow A_2$	$A_2 \leftrightarrow A_2$	$E \leftrightarrow A_2$
perpendicular	(i)	0.61	1.4×10^{-3}	1.3	2.6×10^{-2}	1.1	0.66
perpendicular	(ii)	0.62	2.4×10^{-2}	0.78	1.1	0.72	0.33
parallel	(i)	1.2	3.9×10^{-3}	1.4	8.2×10^{-2}	1.4	1.6
parallel	(ii)	0.33	0.12	0.13	0.20	3.6×10^{-2}	1.6×10^{-2}

[a]The rates for the perpendicular orientation are in [ps^{-1}·nm], while the rates for the parallel orientation are in [ps^{-1}].

different chiralities, owing to the reasons discussed in the previous paragraph.

As we stated before, the phonon-assisted ET rates via process types (i) and (ii) are similar in terms of their mathematical expression. However, the minor differences in the selection rules result in major differences in the behavior of the ET rates via process types (i) and (ii). Figure 3a shows the second-order

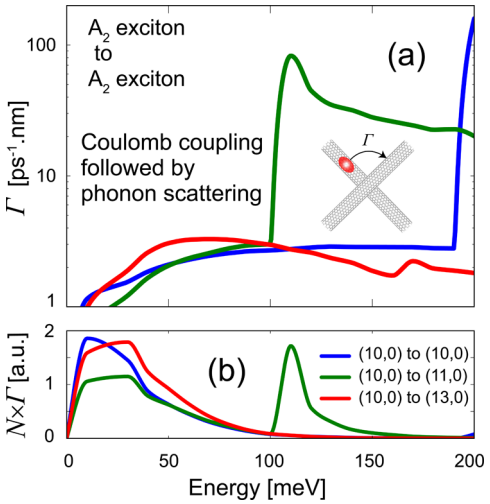

Figure 3. (a) Phonon-assisted ET rates among A_2 excitons in pairs of perpendicular CNTs via process type (ii) (i.e., intertube Coulomb scattering followed by intratube phonon scattering). The energy axis starts from the bottom of the excitonic band in the donor CNT. (b) Phonon-assisted ET rates multiplied by the thermal occupation number at temperature T = 300 K.

ET rates via process (ii) [Coulomb coupling followed by phonon scattering (Figure 1b)]. In all cases (between similar and dissimilar donor and acceptor CNTs), the ET rates tend to zero at the bottom of the exciton energy band. This is due to the shape of the Coulomb coupling matrix element, eq 6, which tends to zero for $\mathbf{K}_1 = 0$ or $\mathbf{K}_2 = 0$. When Coulomb coupling happens first, we have $\mathbf{K}_1 \approx 0$ for the states at the bottom of an excitonic energy band, leading to a zero scattering rate regardless of the band gap in the acceptor CNT. Therefore, the highly populated excitonic states have very small ET rates (Figure 3), which produce lower effective ET rates for process (ii) overall than the rates in process type (i). We also observe a few orders of magnitude jump in the ET rate for process (ii) at the energies that optical phonons become available: $\Omega_{1,s_1}(\mathbf{K}_1) - \min(\Omega_2) = \hbar\omega_{\text{optical}}$. The large jumps are a consequence of the high density of final excitonic states at the bottom of the acceptor−CNT energy band. It is noteworthy that these ET rates are comparable to the intratube exciton relaxation rates due to phonons, and it is therefore possible to observe transfer of hot excitons between CNTs before they are able to relax to lower-energy excitonic states.

First-order ET from the E-type dark excitonic states are at least 2 orders of magnitude lower than the first-order ET from A_2 bright excitonic states.[23] The reason is the weak Coulomb coupling of E-type excitons to any other type of exciton. However, this limitation is overcome in the context of second-order exciton scattering. Figure 4a shows the scattering rates of

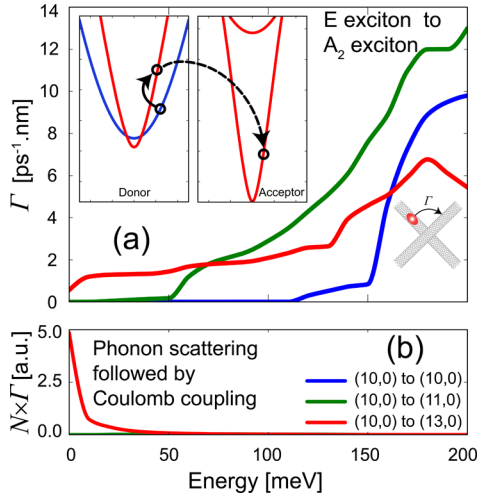

Figure 4. (a) Phonon-assisted ET rates between E and A_2 excitonic states in pairs of perpendicular CNTs. The energy axis starts from the bottom of the excitonic band in the donor CNT. Insets show a schematic of ET mechanism, where first the E-type exciton transitions to an A_2 exciton in the donor CNT via phonon scattering, followed by intertube Coulomb scattering from between A_2 excitonic states in the donor and acceptor CNTs. The solid blue (red) curve shows the dispersion of E-type (A_2) excitons. The solid black arrow indicates exciton−phonon scattering, while the dashed black arrow denotes Coulomb scattering. (b) Phonon-assisted ET rates multiplied by the thermal occupation number at temperature T = 300 K.

E-type excitons in (10,0) CNT to A_2 excitons in acceptor CNTs with various chiralities. If an exciton has enough energy to emit an acoustic or an optical phonon, the transfer rate from dark to bright excitonic states can exceed 1 ps^{-1} nm, about 2 orders of magnitude improvement with respect to the rate of first-order ET between the same excitonic states.[23] As we can see in the insets of Figure 4a, the ET process is of type (i), where in the first step the initial dark excitonic state (E) converts to a bright transition state (A_2) on the same tube via phonon scattering. In the second step, the transition excitonic state couples to the final bright excitonic state via Coulomb interaction.

Unlike the case of ET from the A_2 exciton, the ET rate from low-energy E-type excitons is small even when the acceptor

DOI: 10.1021/acs.jpcc.7b03994
J. Phys. Chem. C 2017, 121, 13084−13091

CNT has a smaller band gap. This behavior can be understood by noting the large difference in angular momentum of *E*-type and A_2 excitons. Therefore, both acoustic and optical phonons that facilitate the second-order ET of *E*-type excitons have a large angular momentum with energies higher than 50 meV. This means that the low-energy excitons can only transfer if the excitonic energy of the acceptor CNT is smaller by more than 50 meV. Among the different choices of sample CNTs we consider here—namely, (10,0), (11,0), and (13,0)—this criterion is satisfied for ET from (10,0) to (13,0), where we observe much higher effective ET rates than for other donor/acceptor CNT pairs (Figure 4b).

3.2. Phonon-Assisted Exciton Transfer Rate for Parallel CNTs. Now, we turn to the case of parallel CNTs, in which the Coulomb matrix element does not depend on the length of the CNTs, but instead it conserves the center-of-mass momentum [eq 10]. In the case of parallel CNTs, the phonon density of states is absent due to the momentum-conservation requirement; therefore, in contrast to the perpendicular case, the phonon-assisted ET rate between parallel tubes does not benefit from the large density of phononic states. However, Coulomb coupling between parallel CNTs is much stronger than the Coulomb coupling between perpendicular CNTs. For example, the first-order ET between parallel CNTs could potentially be 2 orders of magnitude faster (~100 ps^{-1}) than the first-order ET between nonparallel CNTs.[23] However, the number of excitonic states that obey the selection rules is limited for most cases of donor and acceptor CNT chirality, and the first-order ET rate is usually less than 1 ps^{-1}.[23] In second-order exciton scattering, the presence of phonons helps with finding the final excitonic states that obey the selection rules. As phonons increase the number of donor and acceptor exciton states between which an exciton can transfer, the second-order ET rate increases. As we can see in Figure 5a, the exciton scattering rates between bright states generally exceed 1 ps^{-1} regardless of the chirality of donor and acceptor CNTs.

Figure 5b shows the exciton scattering rate from *E*-type excitons to A_2 excitons in pairs of parallel CNTs. The scattering rates have the same trend as the rates in Figure 4a. Again, the scattering rate of low-energy excitons is large when the difference between bottoms of excitonic dispersion energies in donor and acceptor CNTs is large enough to allow for phonon emission.

Overall, the second-order ET rates between parallel CNTs are about 2 orders of magnitude lower that the maximal first-order ET rates between parallel CNTs. However, the second-order process is still relevant since the maximal first-order ET rate only happens for limited choices of donor and acceptor chiralities; the second-order ET rates reported here are faster than the cases of first-order ET process that happen in most experiments.

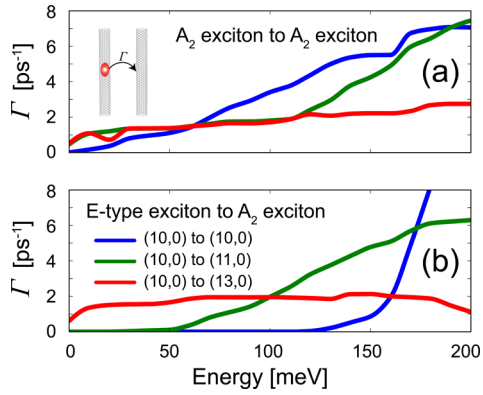

Figure 5. (a) Phonon-assisted ET rates among A_2 excitons in pairs of parallel CNTs. (b) Phonon-assisted ET rates from *E* to A_2 excitonic states in pairs of parallel CNTs. In both panels, process (i) is assumed (intratube phonon scattering, followed by intertube Coulomb scattering). The energy axes start from the bottom of the excitonic band in the donor CNT.

4. CONCLUSIONS

In conclusion, we performed a calculation of second-order phonon-assisted ET between pairs of CNTs with parallel and perpendicular mutual orientations. We showed that the ET rates and the selection rules for the initial and final states are notably different between these two cases. Table 1 shows a summary of the effective ET rates between bright and dark excitonic states of three example CNTs; these effective rates are directly relevant in experiment. The second-order ET rates between bright excitonic states are generally higher than 1 ps^{-1}, which is roughly the same order of magnitude as the first-order ET rates. The second-order ET rate between dark and bright excitonic states can also reach values as high as 1 ps^{-1}, which is about 2 orders of magnitude higher than the first-order ET rates between bright and dark excitons. Dark-exciton transfer is facilitated by exciton scattering with phonons of large angular momentum into same-tube bright states that are strongly Coulomb coupled to bright acceptor-tube states.

These conclusions are true for both parallel and perpendicular tube orientations. The high second-order ET rate between perpendicular CNTs stems from the high density of phononic states. For parallel CNTs, the high ET rate is a result of the selection rules that are much less restrictive in the presence of phonon scattering than for the resonant, first-order Coulomb scattering.

The finding that second-order dark-to-bright exciton transfer is as fast as both first and second order bright-to-bright transfer is very important as a complement to experiments because it shows that dark excitonic states—not directly accessible in experiment—are able to efficiently and directly transfer excitons between CNTs in a CNT film. Together, the fact that second-order bright-to-bright and dark-to-bright exciton transfer has rates on par with first-order resonant transfer is very important for predictive modeling of ET in CNT composites.

AUTHOR INFORMATION

Corresponding Authors

*E-mail: davoody@wisc.edu.

*E-mail: iknezevic@wisc.edu. Phone: (608) 890-3383.

ORCID

M. S. Arnold: 0000-0002-2946-5480

I. Knezevic: 0000-0001-6728-1116

Notes

The authors declare no competing financial interest.

ACKNOWLEDGMENTS

This work was funded by the U.S. Department of Energy (DOE), Office of Basic Energy Sciences, Division of Materials Sciences and Engineering, Physical Behavior of Materials Program, under Award No. DE-SC0008712.

DOI: 10.1021/acs.jpcc.7b03994
J. Phys. Chem. C 2017, 121, 13084−13091

REFERENCES

(1) Liu, Y.; Wang, S.; Peng, L. Toward high-performance carbon nanotube photovoltaic devices. *Adv. Energy Mater.* **2016**, *6*, 1600522.
(2) Shastry, T. A.; Hersam, M. C. Carbon nanotubes in thin-film solar cells. *Adv. Energy Mater.* **2017**, *7*, 1601205.
(3) Depotter, G.; Olivier, J.; Glesner, M. G.; Deria, P.; Bai, Y.; Bullard, G.; Kumbhar, A.; Therien, M. J.; Clays, K. First-order hyperpolarizabilities of chiral, polymer-wrapped single-walled carbon nanotubes. *Chem. Commun.* **2016**, *52*, 12206−12209.
(4) Jariwala, D.; Sangwan, V. K.; Lauhon, L. J.; Marks, T. J.; Hersam, M. C. Carbon nanomaterials for electronics, optoelectronics, photovoltaics, and sensing. *Chem. Soc. Rev.* **2013**, *42*, 2824−2860.
(5) Arnold, M. S.; Blackburn, J. L.; Crochet, J. J.; Doorn, S. K.; Duque, J. G.; Mohite, A.; Telg, H. Recent developments in the photophysics of single-walled carbon nanotubes for their use as active and passive material elements in thin film photovoltaics. *Phys. Chem. Chem. Phys.* **2013**, *15*, 14896−14918.
(6) Jain, R. M.; Howden, R.; Tvrdy, K.; Shimizu, S.; Hilmer, A. J.; McNicholas, T. P.; Gleason, K. K.; Strano, M. S. Polymer-free near-infrared photovoltaics with single chirality (6,5) semiconducting carbon nanotube active layers. *Adv. Mater.* **2012**, *24*, 4436−4439.
(7) Bindl, D. J.; Safron, N. S.; Arnold, M. S. Dissociating excitons photogenerated in semiconducting carbon nanotubes at polymeric photovoltaic heterojunction interfaces. *ACS Nano* **2010**, *4*, 5657−5664.
(8) Bindl, D. J.; Wu, M.-Y.; Prehn, F. C.; Arnold, M. S. Efficiently harvesting excitons from electronic type-controlled semiconducting carbon nanotube films. *Nano Lett.* **2011**, *11*, 455−460.
(9) Bindl, D. J.; Brewer, A. S.; Arnold, M. S. Semiconducting carbon nanotube/fullerene blended heterojunctions for photovoltaic near-infrared photon harvesting. *Nano Res.* **2011**, *4*, 1174−1179.
(10) Bindl, D. J.; Shea, M. J.; Arnold, M. S. Enhancing extraction of photogenerated excitons from semiconducting carbon nanotube films as photocurrent. *Chem. Phys.* **2013**, *413*, 29−34.
(11) Soavi, G.; Scotognella, F.; Lanzani, G.; Cerullo, G. Ultrafast photophysics of single-walled carbon nanotubes. *Adv. Opt. Mater.* **2016**, *4*, 1670−1688.
(12) Bellisario, D. O.; Jain, R. M.; Ulissi, Z.; Strano, M. S. Deterministic modelling of carbon nanotube near-infrared solar cells. *Energy Environ. Sci.* **2014**, *7*, 3769−3781.
(13) Koyama, T.; Miyata, Y.; Asaka, K.; Shinohara, H.; Saito, Y.; Nakamura, A. Ultrafast energy transfer of one-dimensional excitons between carbon nanotubes: a femtosecond time-resolved luminescence study. *Phys. Chem. Chem. Phys.* **2012**, *14*, 1070−1084.
(14) Maeda, A.; Matsumoto, S.; Kishida, H.; Takenobu, T.; Iwasa, Y.; Shimoda, H.; Zhou, O.; Shiraishi, M.; Okamoto, H. Gigantic optical Stark effect and ultrafast relaxation of excitons in single-walled carbon nanotubes. *J. Phys. Soc. Jpn.* **2006**, *75*, 043709.
(15) Koyama, T.; Asaka, K.; Hikosaka, N.; Kishida, H.; Saito, Y.; Nakamura, A. Ultrafast exciton energy transfer in bundles of single-walled carbon nanotubes. *J. Phys. Chem. Lett.* **2010**, *2*, 127−132.
(16) Berger, S.; Voisin, C.; Cassabois, G.; Delalande, C.; Roussignol, P. Temperature dependence of exciton recombination in semiconducting single-wall carbon nanotubes. *Nano Lett.* **2007**, *7*, 398−402.
(17) Qian, H.; Georgi, C.; Anderson, N.; Green, A. A.; Hersam, M. C.; Novotny, L.; Hartschuh, A. Exciton energy transfer in pairs of single-walled carbon nanotubes. *Nano Lett.* **2008**, *8*, 1363−1367.
(18) Lüer, L.; Crochet, J.; Hertel, T.; Cerullo, G.; Lanzani, G. Ultrafast excitation energy transfer in small semiconducting carbon nanotube aggregates. *ACS Nano* **2010**, *4*, 4265−4273.
(19) Mehlenbacher, R. D.; Wu, M. Y.; Grechko, M.; Laaser, J. E.; Arnold, M. S.; Zanni, M. T. Photoexcitation dynamics of coupled semiconducting carbon nanotube thin films. *Nano Lett.* **2013**, *97*, 1495.
(20) Grechko, M.; Ye, Y.; Mehlenbacher, R. D.; McDonough, T. J.; Wu, M. Y.; Jacobberger, R. M.; Arnold, M. S.; Zanni, M. T. Diffusion-assisted photoexcitation transfer in coupled semiconducting carbon nanotube thin films. *ACS Nano* **2014**, *8*, 5383−5394.
(21) Mehlenbacher, R. D.; McDonough, T. J.; Grechko, M.; Wu, M.-Y.; Arnold, M. S.; Zanni, M. T. Energy transfer pathways in semiconducting carbon nanotubes revealed using two-dimensional white-light spectroscopy. *Nat. Commun.* **2015**, *6*, 6732.
(22) Mehlenbacher, R. D.; Wang, J.; Kearns, N. M.; Shea, M. J.; Flach, J. T.; McDonough, T. J.; Wu, M. Y.; Arnold, M. S.; Zanni, M. Ultrafast exciton hopping oObserved in bare semiconducting carbon nanotube thin films with 2DWL spectroscopy. *J. Phys. Chem. Lett.* **2016**, *7*, 2024−2031.
(23) Davoody, A. H.; Karimi, F.; Arnold, M. S.; Knezevic, I. Theory of exciton energy transfer in carbon nanotube composites. *J. Phys. Chem. C* **2016**, *120*, 16354−16366.
(24) Yang, M.; Fleming, G. R. Influence of phonons on exciton transfer dynamics: comparison of the Redfield, Förster, and modified Redfield equations. *Chem. Phys.* **2002**, *275*, 355−372.
(25) Chou, S. G.; DeCamp, M. F.; Jiang, J.; Samsonidze, G. G.; Barros, E. B.; Plentz, F.; Jorio, A.; Zheng, M.; Onoa, G. B.; Semke, E. D.; Tokmakoff, A.; Saito, R.; Dresselhaus, G.; Dresselhaus, M. S. Phonon-assisted exciton relaxation dynamics for a (6,5)-enriched DNA-wrapped single-walled carbon nanotube sample. *Phys. Rev. B: Condens. Matter Mater. Phys.* **2005**, *72*, 195415.
(26) Rozbicki, E.; Machnikowski, P. Quantum kinetic theory of phonon-assisted excitation transfer in quantum dot molecules. *Phys. Rev. Lett.* **2008**, *100*, 027401.
(27) Nazir, A. Correlation-dependent coherent to incoherent transitions in resonant energy transfer dynamics. *Phys. Rev. Lett.* **2009**, *103*, 146404.
(28) Gilmore, J. B.; McKenzie, R. H. Criteria for quantum coherent transfer of excitations between chromophores in a polar solvent. *Chem. Phys. Lett.* **2006**, *421*, 266−271.
(29) Rebentrost, P.; Mohseni, M.; Kassal, I.; Lloyd, S.; Aspuru-Guzik, A. Environment-assisted quantum transport. *New J. Phys.* **2009**, *11*, 033003.
(30) Zimanyi, E. N.; Silbey, R. J. Theoretical description of quantum effects in multi-chromophoric aggregates. *Philos. Trans. R. Soc., A* **2012**, *370*, 3620−3637.
(31) Govorov, A. O. Spin-Förster transfer in optically excited quantum dots. *Phys. Rev. B: Condens. Matter Mater. Phys.* **2005**, *71*, 155323.
(32) Postupna, O.; Jaeger, H. M.; Prezhdo, O. V. Photoinduced dynamics in carbon nanotube aggregates steered by dark excitons. *J. Phys. Chem. Lett.* **2014**, *5*, 3872−3877.
(33) Jiang, J.; Saito, R.; Samsonidze, G. G.; Jorio, A.; Chou, S. G.; Dresselhaus, G.; Dresselhaus, M. S. Chirality dependence of exciton effects in single-wall carbon nanotubes: Tight-binding model. *Phys. Rev. B: Condens. Matter Mater. Phys.* **2007**, *75*, 035407.
(34) Rohlfing, M.; Louie, S. G. Electron-hole excitations and optical spectra from first principles. *Phys. Rev. B: Condens. Matter Mater. Phys.* **2000**, *62*, 4927−4944.
(35) Tayo, B. O.; Rotkin, S. V. Charge impurity as a localization center for singlet excitons in single-wall nanotubes. *Phys. Rev. B: Condens. Matter Mater. Phys.* **2012**, *86*, 125431.
(36) Su, W. P.; Schrieffer, J. R.; Heeger, A. J. Soliton excitations in polyacetylene. *Phys. Rev. B: Condens. Matter Mater. Phys.* **1980**, *22*, 2099−2111.
(37) Perebeinos, V.; Tersoff, J.; Avouris, P. Effect of exciton-phonon coupling in the calculated optical absorption of carbon nanotubes. *Phys. Rev. Lett.* **2005**, *94*, 027402.
(38) Chang, J. C. Monopole effects on electronic excitation interactions between large molecules. I. Application to energy transfer in chlorophylls. *J. Chem. Phys.* **1999**, *67*, 3901−3909.
(39) Wong, C. Y.; Curutchet, C.; Tretiak, S.; Scholes, G. D. Ideal dipole approximation fails to predict electronic coupling and energy transfer between semiconducting single-wall carbon nanotubes. *J. Chem. Phys.* **2009**, *130*, 081104.
(40) Sakurai, J. J.; Napolitano, J. *Modern quantum mechanics*; Pearson: New York City, 2011.
(41) Jiang, J.; Saito, R.; Samsonidze, G. G.; Chou, S. G.; Jorio, A.; Dresselhaus, G.; Dresselhaus, M. S. Electron-phonon matrix elements

DOI: 10.1021/acs.jpcc.7b03994
J. Phys. Chem. C 2017, 121, 13084−13091

in single-wall carbon nanotubes. *Phys. Rev. B: Condens. Matter Mater. Phys.* **2005**, *72*, 235408.
(42) Saito, R.; Dresselhaus, G.; Dresselhaus, M. S. *Physical properties of carbon nanotubes*; Imperial College Press: London, 1998.
(43) Davoody, A. H. Dynamics of electronic excitations in carbon nanotube composites. *PhD Dissertation* University of Wisconsin - Madison, 2016.
(44) Toyozawa, Y. Theory of line-shapes of the exciton absorption bands. *Prog. Theor. Phys.* **1958**, *20*, 53−81.
(45) Segall, B.; Mahan, G. Phonon-assisted recombination of free excitons in compound semiconductors. *Phys. Rev.* **1968**, *171*, 935−948.

DOI: 10.1021/acs.jpcc.7b03994
J. Phys. Chem. C 2017, 121, 13084−13091